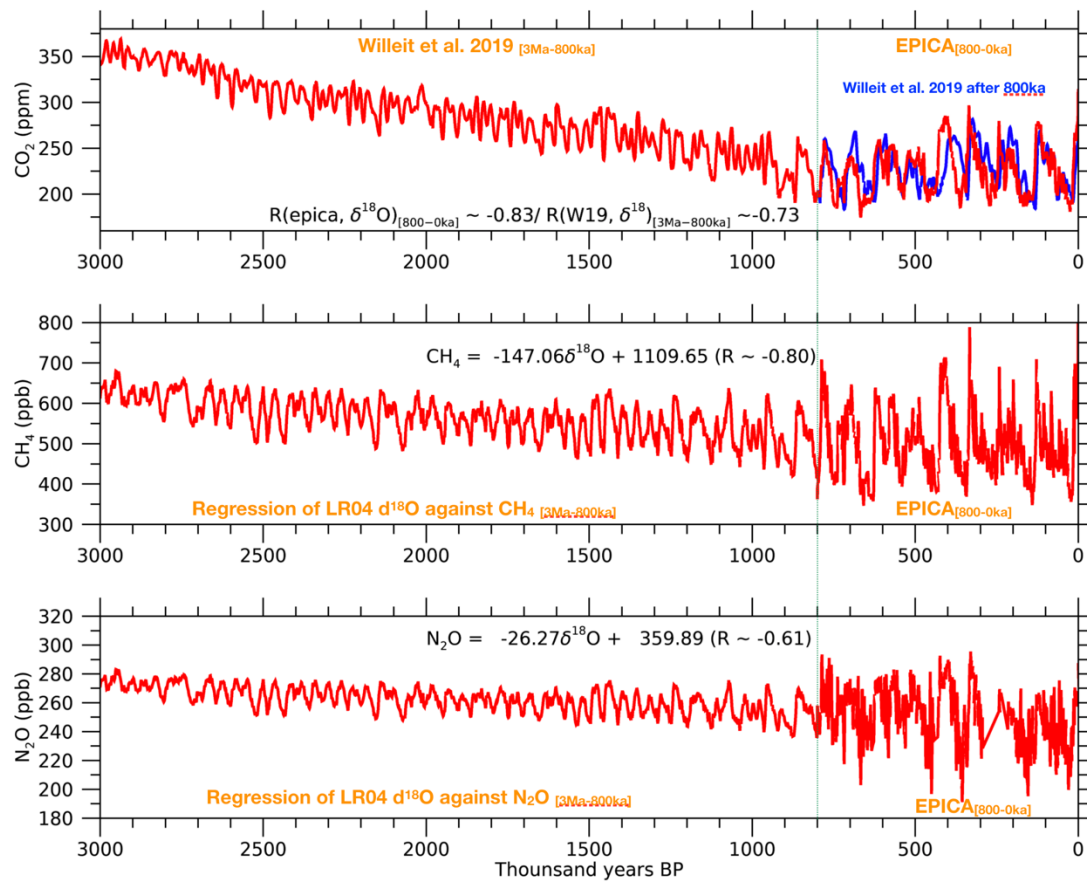Climate
of the Past

Open Access

EGU

Supplement of

A transient coupled general circulation model (CGCM) simulation of the past 3 million years

Kyung-Sook Yun et al.

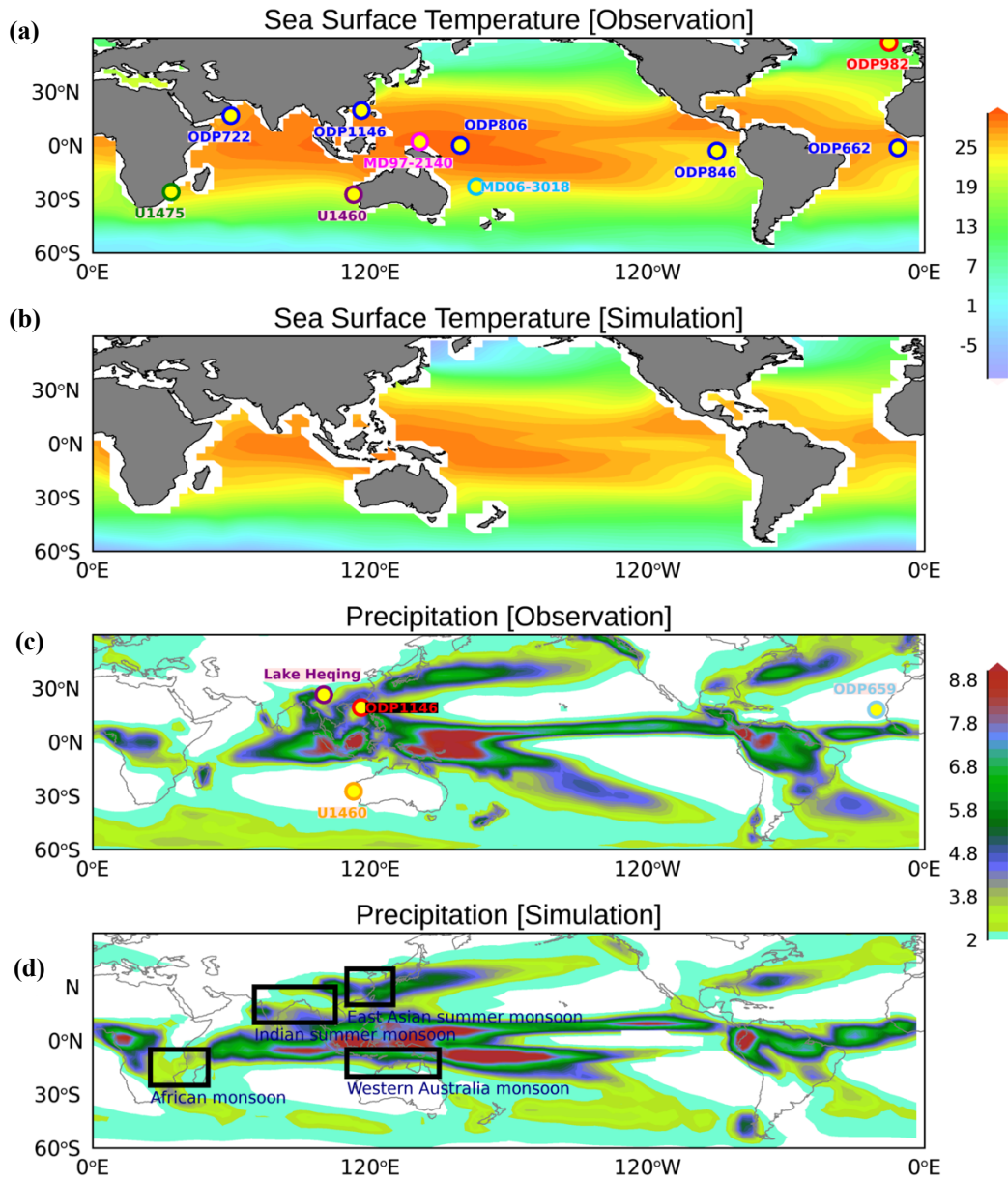*Correspondence to:* Kyung-Sook Yun (kssh@pusan.ac.kr) and Axel Timmermann (axel@ibsclimate.org)

Figure S1 | Greenhouse-gases forcing. (a) Reconstructed CO_2 forcing (red) by combining two datasets of the European Project for Ice Coring in Antarctica (EPICA) Dome ice core data (Lüthi et al. 2008) after 800ka and Willeit et al. (2019) before 800ka. Blue line indicates the CO_2 forcing from Willeit et al. (2019). (b-c) Reconstructed (b) CH_4 and (c) N_2O forcings by combining two datasets of EPICA CH_4 (Loulergue et al. 2008) and N_2O (Spahni et al. 2005) data after 800ka and regression model before 800ka. Here, the regression was conducted using the linear relationship between LR04 stack (Lisiecki and Raymo 2005) and the greenhouse-gases during the EPICA 800 kyr. The regression coefficients were displayed by equation of each panel.

(a) Sea Surface Temperature [Observation]

(b) Sea Surface Temperature [Simulation]

(c) Precipitation [Observation]

(d) Precipitation [Simulation]

Figure S2 | SST and precipitation pattern. (a) Observed SST pattern during 1979-2008 from ERSST5 and proxy locations used in this study. (b) Simulated SST pattern over the entire 3Myr. (c) Observed precipitation pattern during 1979-2008 from GPCP and proxy locations. (d) Simulated precipitation pattern over the 3Myr and monsoon domains used in this study.

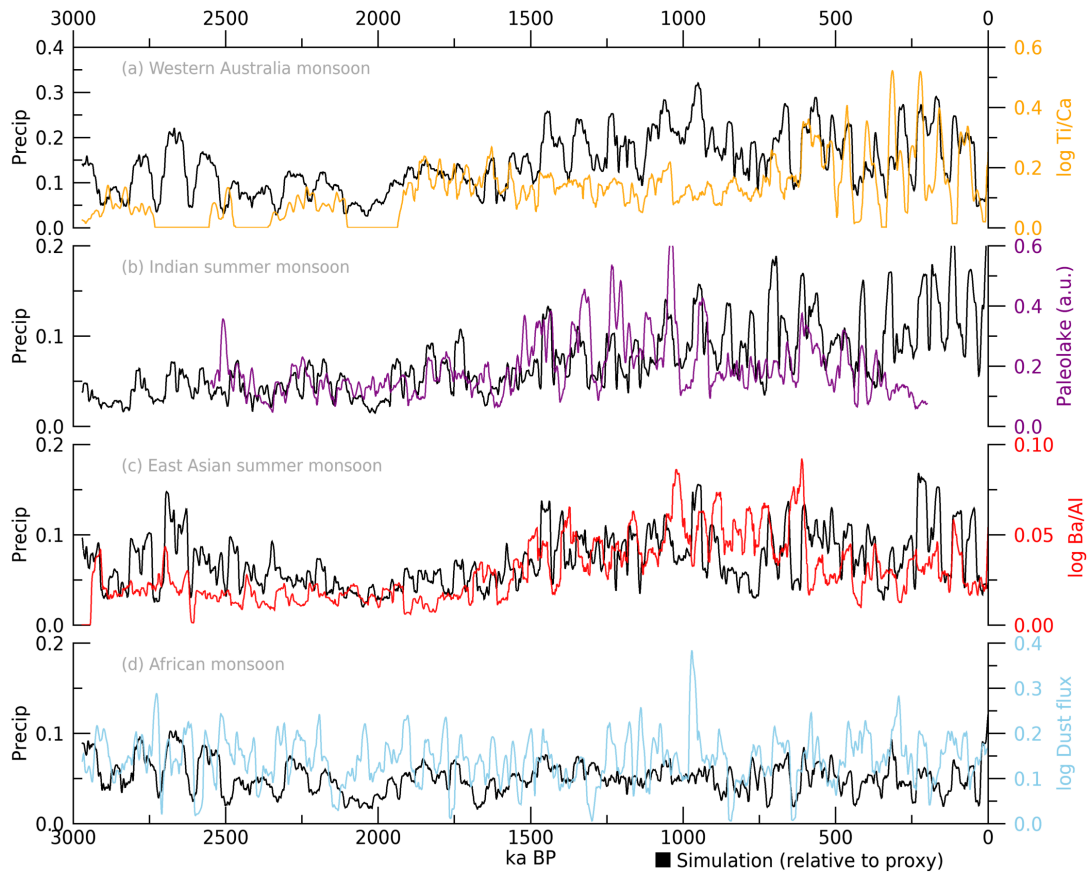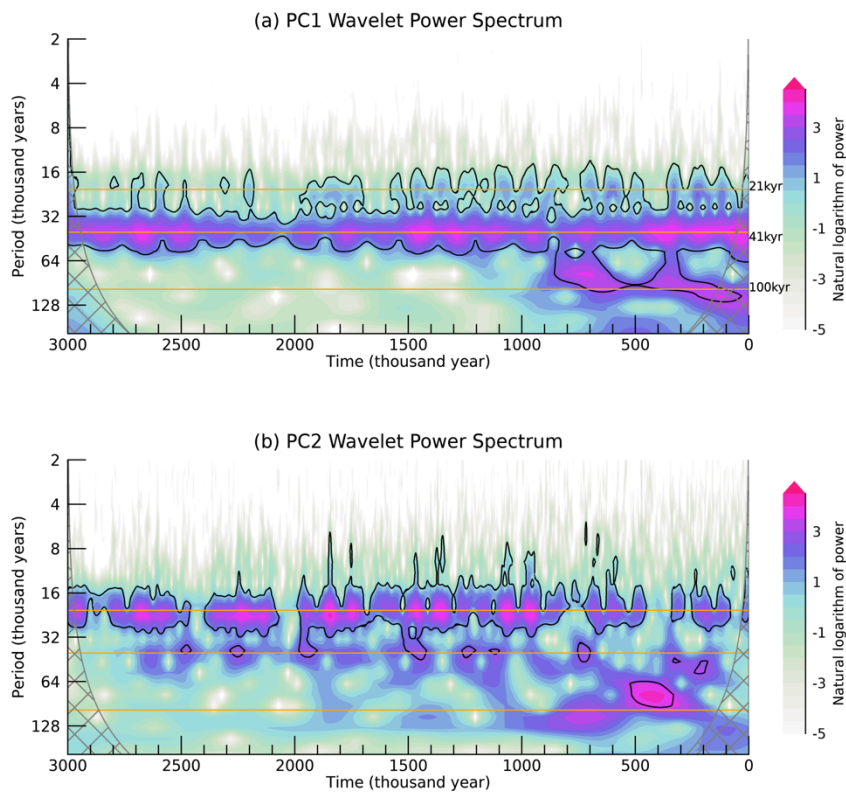**Figure S3 | Changes in monsoon variability amplitude.** Sliding standard deviation of precipitation (unit: mm d⁻¹) and proxies over 31-kyr time window: (a) Western Australia monsoon from simulation averaged over 20°S-5°S, 110°E-150°E (black) and from proxies of IODP site U1460 log Ti/Ca (Petrick et al. 2019; orange); (b) Indian summer monsoon from simulation averaged over 10°N-30°N, 70°E-105°E (black) and from proxies of Lake Heqing (An et al. 2011; purple); (c) East Asian summer monsoon from simulation averaged over 20°N-40°N, 110°E-130°E (black) and from proxies of ODP 1146 log Ba/Al (Clemens et al. 2008; red); (d) western African monsoon from simulation averaged over 25°S-5°S, 25°E-50°E (black) and from proxies of ODP 659 log Dust flux (Tiedemann et al. 1994; sky blue).

39
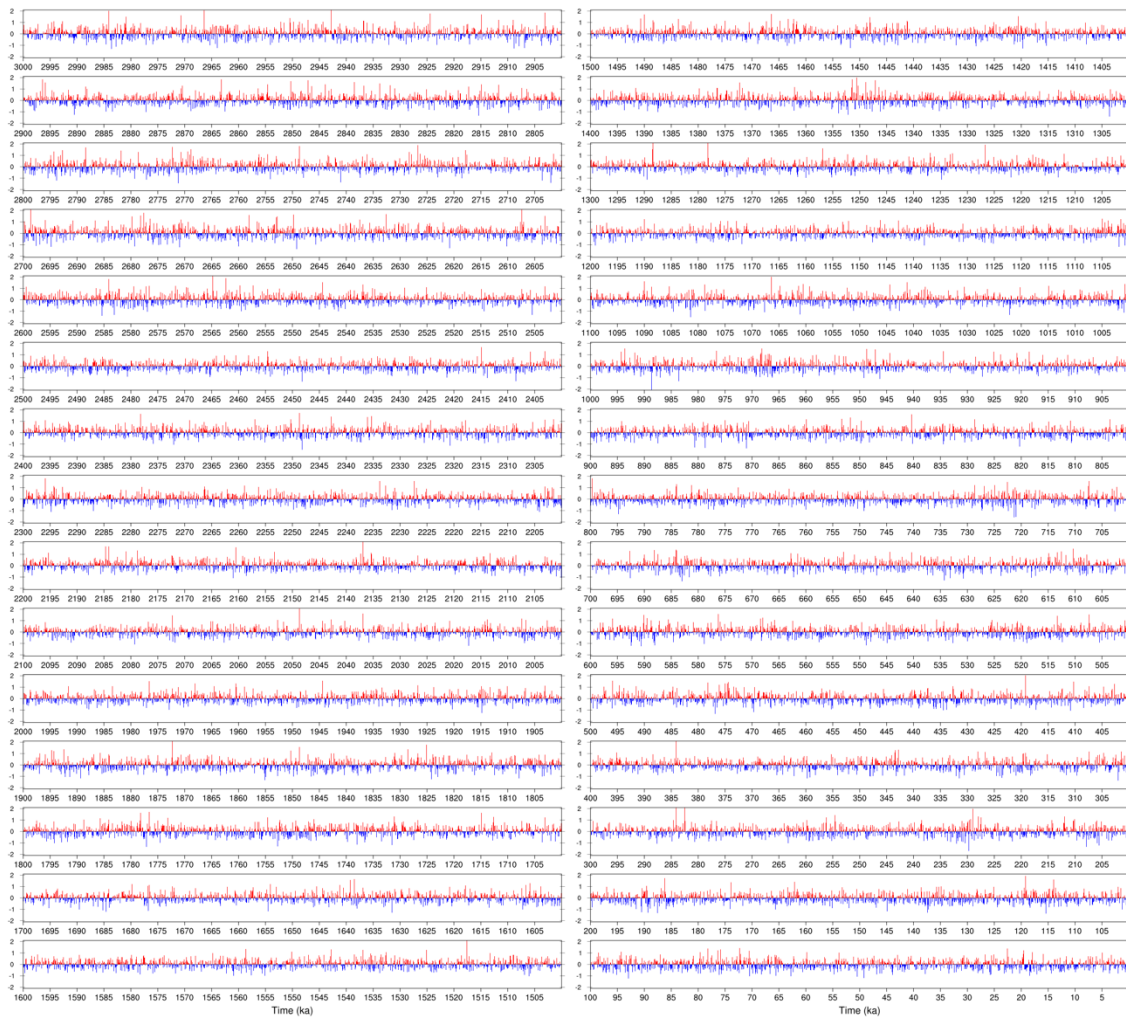
**Figure S4 | Monthly ENSO variability.** Timeseries of Niño 3 index defined as 1.5-7-year band-pass

41 filtered Niño 3 SST.

42

43

44 **Figure S5 | Wavelet power spectrum of PCs of two dominant MHT modes.** The wavelet power spectrum

45 of (a) PC1, and (b) PC2. The black contour indicates the value significant at the 95% confidence level. The

46 horizonal orange lines show 21-kyr (precession), 41-kyr (obliquity), and 100-kyr (eccentricity) periods.

47

48

49
50
51
52
53
54
55
56
57
58
59
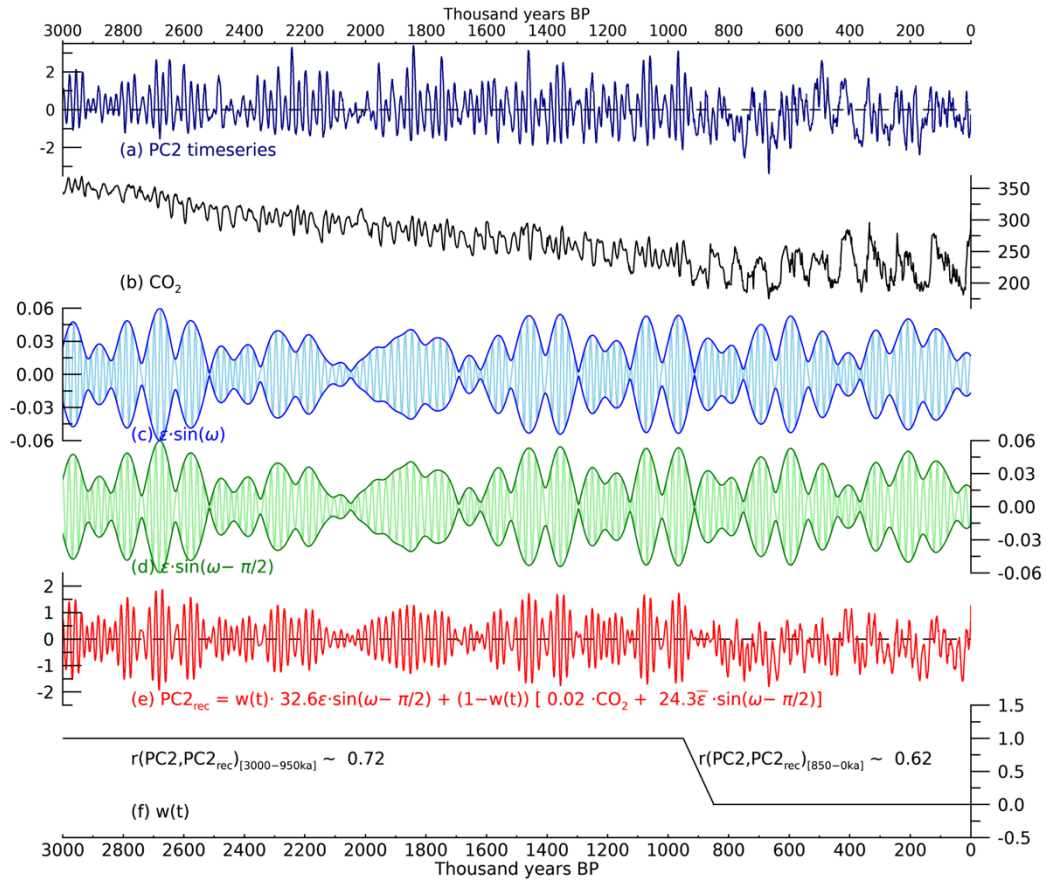
Figure S6 | A simple model for reconstruing PC2 time series using eccentricity-modulated precession and CO_2. (a) Original PC2 time series, (b) CO_2 forcing, (c) eccentricity (blue)-modulated precession (sky blue) variability. (d) 90° out-of-phase precession variability, (e) reconstructed PC2 time series using 90° out-of-phase precession and CO_2 forcing, and (f) weight function in the reconstruction. The coefficients in (e) are obtained using a simple regression model against the PC2 time series.
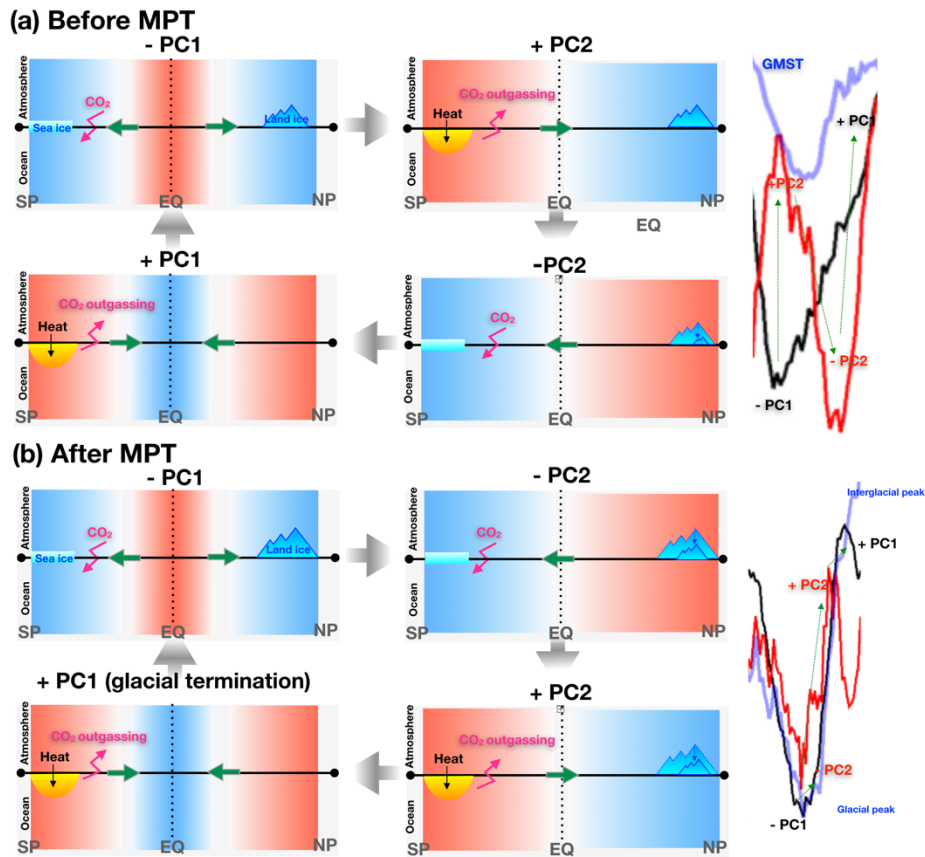
Figure S7 | PC1-PC2 cycle and the potential feedback with carbon cycle. The cycle of PC1 and PC2 (a) before the MPT and (b) after the MPT. Before the MPT, the negative PC1 tends to be followed by the positive PC2 and it becomes the other way around. Meanwhile, after the MPT, the negative PC1 tends to be followed by the negative PC2 during the glacial peak. The transition into positive phases of PC2 and PC1 is concurrent with the glacial termination. The negative phases of PC1 and PC2 are likely to enhance the Southern Ocean CO_2 sequestration into the ocean, associated with the sea ice/carbon cycle feedback (Stein et al. 2020). By contrast, the positive phases of PC1 and PC2 are related to the Southern Ocean warming and the enhanced CO_2 leak outgoing into the atmosphere. Here, blue (red) shading and green arrow show an anomalous cooling (warming) and direction of heat transport.

90   **References**

91   An, Z., and Coauthors, 2011: Glacial-Interglacial Indian Summer Monsoon Dynamics.

92   *Science*, **333,** 719-723.

93   Clemens, S. C., W. L. Prell, Y. Sun, Z. Liu, and G. Chen, 2008: Southern Hemisphere

94   forcing of Pliocene δ18O and the evolution of Indo-Asian monsoons. *Paleoceanography*,

95   **23**.

96   Lisiecki, L. E., and M. E. Raymo, 2005: A Pliocene-Pleistocene stack of 57 globally

97   distributed benthic δ18O records. *Paleoceanography*, **20**.

98   Loulergue, L., and Coauthors, 2008: Orbital and millennial-scale features of atmospheric

99   CH4 over the past 800,000 years. *Nature*, **453,** 383-386.

100   Lüthi, D., and Coauthors, 2008: High-resolution carbon dioxide concentration record

101   650,000–800,000 years before present. *Nature*, **453,** 379-382.

102   Petrick, B., and Coauthors, 2019: Glacial Indonesian Throughflow weakening across the

103   Mid-Pleistocene Climatic Transition. *Sci Rep-Uk*, **9,** 16995.

104   Spahni, R., and Coauthors, 2005: Atmospheric Methane and Nitrous Oxide of the Late

105   Pleistocene from Antarctic Ice Cores. *Science*, **310,** 1317-1321.

106   Stein, K., A. Timmermann, E. Y. Kwon, and T. Friedrich, 2020: Timing and magnitude of

107   Southern Ocean sea ice/carbon cycle feedbacks. *Proceedings of the National Academy of*

108   *Sciences*, **117,** 4498-4504.

109   Tiedemann, R., M. Sarnthein, and N. J. Shackleton, 1994: Astronomic timescale for the

110   Pliocene Atlantic δ18O and dust flux records of Ocean Drilling Program Site 659.

111   *Paleoceanography*, **9,** 619-638.

112   Willeit, M., A. Ganopolski, R. Calov, and V. Brovkin, 2019: Mid-Pleistocene transition

113   in glacial cycles explained by declining CO2 and regolith removal. *Sci Adv*, **5**.

114